RSC Advances

RSC Advances

www.rsc.org/advances

ROYAL SOCIETY OF CHEMISTRY

www.rsc.org/advances

Novel Approach to Synthesis Polymer-Functionalized Fe$_3$O$_4$/SiO$_2$-NH$_2$ *via* Ultrasonic-Assisted Method as a Catalyst to Selective Oxidation of Alcohols to Aldehydes and Ketones in the Mixture of DMSO and Water

Mahsa Dehghan[b], Atieh Motaharinejad[c], Mostafa Saadat[d], Reza Ahdenov[a], Mirzaagha Bab azadeh[a],* and Rahim Hosseinzadeh-Khanmiri[a]

[a]*Department of Chemistry, Tabriz Branch, Islamic Azad University, Tabriz, Iran. E-mail: babazadeh@iaut.ac.ir, Fax: +98-491-2231616*
[b]*Department of Organic Chemistry, Faculty of Chemistry, Razi University, Kermanshah 67149-67346, Iran*
[c]*Department of physical chemistry, Faculty of chemistry, Kashan University, Kashan, Iran*
[d]*Department of Chemistry, Faculty of Science, Urmia University, Urmia 57154, Iran*

Abstract

N-(2-oxotetrahydrothiophen-3-yl)acrylamide was successfully polymerized onto surface of amine functionalized magnetic silica nanocomposites *via* ultrasonic-assisted method. Then, MnO$_2$ nanoparticles were formed on surface of polymer functionalized magnetic nanocomposites leading to a magnetically recoverable MNO$_2$ catalyst, which exhibits high catalytic activity in the selective aerobic oxidation of alcohols to aldehydes and ketones in the mixture of DMSO and water in 30 min. The catalyst can be separated from the reaction mixture by applying a permanent magnet externally and can be reused for several times without significant loss of activity.

Keywords: Polymer, Ultrasonic, Magnetic Silica Nanocomposites, MnO$_2$, Aerobic Oxidation.

1. Introduction

Nanoscience and nanotechnology have attracted great interest from the scientific community due to the new technological possibilities offered by the properties of nanomaterials.[1] A wide variety of applications have been suggested, in field ranging from electronic,[2] nanocatalysis,[3,4] magnetite-supported catalysis,[5] *etc*. Rapid development of nanotechnology over the past few decades has allowed researchers to view conventional heterogeneous catalysts from a new perspective. In particular, catalytic materials can now be prepared with greater precision via nanotech-enabled processes. Combining properties of NPs with polymers, aiming at the

production of hybrid multifunctional nanoparticles (NPs) and nanostructures, presents several advantages and opportunities.[6] Hybrid NPs containing polymer, which often serve as active catalytic components, can now be routinely synthesized with well-defined sizes, shapes, crystal facets, structure and composition.[7] Such controllability over materials' structures could potentially lead to the development of new technologies for applications in green, sustainable and economically-viable chemical processes, which are currently regarded as among the most desirable yet challenging areas in chemistry.

Magnetic nanomaterials stand out for their novel properties.[8] The most widely studied superparamagnetic NPs is magnetite (Fe_3O_4), which offers a large variety of applications, such as information storage,[9] color imaging,[10] microwave absorption,[11] medical diagnosis,[12] catalyst,[13] and so on. However, naked Fe_3O_4 NPs are very sensitive to oxidation for their high chemical reactivities and prone to aggregate for their large ratio of surface area to volume and thus result in poor magnetism and dispersibility. Those defects limit their further applications. One of the main approaches to overcome these limitations is to protect naked magnetic NPs with polymers or inorganic shell such as metals or oxides.[14] These protective layers not only prevent the Fe3O4 NPs from aggregating but also provide a useful platform for further functionalization. Several ways for the functionalization of this hybrid nanomaterials have been reported, for example immobilization of metal,[15] anchoring the organic species, reducing metal ion onto the surface of the nanocomposites via different methods.[16,17] Three-component magnetic nanocomposites have been paid much attention. Stoeva et al. assembled magnetic NPs into a core/shell/shell structure with a silica core with Fe_3O_4 and gold as the inner and outer shells, respectively.[18] These core/shell/shell magnetic NPs have excellent DNA binding properties as well as magnetic properties. Yu et al. prepared Fe_3O_4@Au/polyaniline (PANI) nanocomposites by in situ polymerization in the presence of mercaptocarboxylic acid with integrated and stable optical, electrical, and magnetic properties.[19] These species of nanocomposites exhibited promising application in many catalytic process.

Selective oxidation of alcohols to their corresponding carbonyl compounds is of significant importance in organic chemistry, both for fundamental research and industrial manufacturing. This transformation is traditionally carried out using stoichiometric quantities of inorganic oxidants, which are relatively expensive, highly toxic and environmentally polluting.[20] Therefore, introducing green, selective and efficient aerobic oxidation systems for alcohols are of

prime importance for both economic and environmental reasons. From both environmental and economic viewpoints, heterogeneous catalysts have attracted considerable interest for catalytic systems.[21] Various materials have been employed as the support to produce heterogeneous catalytic systems, such as mesoporous silica,[22] activated carbon,[23] (bio)polymer and biomass.[24]

In this paper, a new kind of three-component magnetic nanocomposite, $Fe_3O_4/SiO_2/PATL$ was synthesized. First, uniform Fe_3O_4 nanospheres with a diameter of 10 nm were prepared. Then, $Fe_3O_4/SiO_2{\sim}NH_2$ nanospheres with well-defined core/shell nanocomposite structures were obtained through polymerization of (3-Aminopropyl)triethoxysilane (APTES) over the group of Fe_3O_4 NPs. Finally, N-(2-oxotetrahydrothiophen-3-yl)acrylamide (ATL) was polymerized onto the surface of the $Fe_3O_4/SiO_2{\sim}NH_2$. The obtained three-component magnetic nanocomposite was used to immobilizing of MnO_2 nanoparticles as heterogeneous catalyst for selective oxidation of alcohols.

2. Experimental Section

Iron(III) chloride hexahydrate ($FeCl_3{\cdot}6H_2O$), (3-Aminopropyl)triethoxysilane (99%), DL-homocysteine thiolactone hydrochloride (CTH), acryloyl chloride, methacryloyl chloride, dimethylphenylphosphine (DPP) and all amines were purchased from Sigma-Aldrich and used as received.

2.1. Preparation of organosilica coated magnetite NPs ($Fe_3O_4/SiO_2–NH_2$)

Magnetite (Fe_3O_4) nanoparticles (NPs) were prepared according to the reported method (co-precipitation) and coated with organosilane in the presence of 2-propanol (sol–gel method). In brief, 0.036 mol of $FeCl_3.6H_2O$ and 0.018 mol of $FeCl_2.4H_2O$ were dissolved in 20 mL deionized water under nitrogen gas with vigorous stirring. Then, NH_3 (25%) was added into the solution until the pH of the solution reached. Stirring was continued for 1 h at 60 ^{o}C. The color of the bulk solution turned from orange to black immediately. The magnetite precipitate was separated from the solution using a magnet, washed several times with deionized water and ethanol, and left to dry in air. Then, the obtained MNP powder (300 mg) was dispersed in 2-propanol (150 mL) and water (15 mL) by sonication before APTES (99%, 120 µL) was added to the mixture. After mechanically agitation for 7 h, the suspended substance was separated from the solution using a magnet. The settlement product was re-dispersed in ethanol by sonication and isolated

with magnetic decantation for 5 times. The precipitated product ($Fe_3O_4/SiO_2–NH_2$) was dried at room temperature under vacuum.

2.2. Preparation of $Fe_3O_4/SiO_2/PATL$ nanocomposites.

N-(2-oxotetrahydrothiophen-3-yl)acrylamide (ATL) was synthesized according to previously reported by the amidation of DL-homocysteine thiolactone hydrochloride with acryloyl chloride in dichloromethane (DCM) using triethylamine (TEA) as base. Then, to solution of 17.1 mg (0.1 mmol) ATL and 0.05 equivalent DPP (0.70 mg, 0.005 mmol) in 5 mL of ethanol, 300 mg of $Fe_3O_4/SiO_2–NH_2$ was added and the mixture was sonicated at r.t. for 2 h. Finally, the precipitated solid was separated using external magnet and several time washed by ethanol. The precipitated product ($Fe_3O_4/SiO_2/PATL$) was dried at 80 ^{o}C for 12 h.

2.3. Preparation of MnO_2 NPs on surface of $Fe_3O_4/SiO_2/PATL$ nanocmposites.

A mixture of $Fe_3O_4/SiO_2/PATL$ (1.00 g) in 20 mL of H_2O at 60 °C, a solution of $KMnO_4$ (0.01 M, 80 mL) at 60 °C, and a solution of $MnCl_2$ (0.02 M, 60 mL) at 70 °C were prepared, separately. In continue, the solutions of $KMnO_4$ and $MnCl_2$ were added dropwise to the mixture of $Fe_3O_4/SiO_2/PATL$ for 12 h at 60 °C. The mixture was stirred at room temperature; after 24 h, it was separated using external magnet, and the residue ($Fe_3O_4/SiO_2/PATL/MnO_2$) washed successively with H_2O (3 × 5 mL) and EtOH (3 × 10 mL) and dried at 80 °C. The loading of manganese was measured to be 0.80 mmol g^{-1} by inductively coupled plasma-optical emission spectrometry (ICP-OES).

2.4. Characterization techniques

Infrared spectra were recorded using a Ray Leigh Wqf-510 fourier transform infrared (FTIR) spectrophotometer. Morphological studies measurements were performed using a transition electron microscopy (TEM, Philips CM10) operated at an 80 kV electron beam accelerating voltage. Scanning electron microscopy (SEM) and EDX were performed on a PhilipsXL-300 instrument. The sample was sputtered by gold to avoid undesirable electron charging. X-ray diffraction was conducted using a Philips X'pert Pro (PW 3040) X-ray diffractometer with monochromatic Cu-Karadiation (k¼1.54056˚ A, 40 kV, 30 mA). Thermogravimetric analyses were investigated using a TG/DTA6300 instrument, at a heating rate of 20 ^{o}C min^{-1} under nitrogen flow. Elemental analysis was performed with a CHN machine (Perkin Elmer Series II,

2400). The concentration of manganese was estimated using Shimadzu AA-680 flame atomic absorption spectrophotometer and inductively coupled plasma optical emission spectrometer (ICP-OES) Varian Vista PRO Radial.

2.5. Oxidation of alcohols in presence of $Fe_3O_4/SiO_2/PATL/MnO_2$; General procedure

In a general process, an alcohol (1 mmol) was added to a two-necked flask containing $Fe_3O_4/SiO_2/PATL/MnO_2$ (0.06 g, 4.8 mol%), K_2CO_3 (0.5 mmol) and mixture 1:1(v/v) of DMSO:deionized water (5 mL). The reaction mixture was stirred under air blowing for 30-50 min at room temperature. The progress of the reaction was followed by thin layer chromatography (TLC). Upon completion, the catalyst was collected using external magnet and the reaction solution was analyzed by GC method.

3. Results and discussion

3.1. Preparation and characterization of the catalyst

The $Fe_3O_4/SiO_2/PATL/MnO_2$ nanocatalyst was prepared with a multi-step reaction, initially by preparing iron oxide as a magnetic core for coating by organosilica through sol-gel method. It is known that organosilanes can act as a linker between the organic catalyst and the support. In this work, APTES was used. Scheme 1 illustrates the process of catalyst preparation. The ATL (monomer) was synthesized according to previously reported by the amidation of $_{DL}$-homocysteine thiolactone hydrochloride with acryloyl chloride.[25] The polymerization was carried out by thiobutyr-olactone aminolysis via a part of the linker's amine and consequent thiol-(meth)acrylate addition. Finally, MnO_2 NPs was formed onto surface of nanocomposites through the reaction of $KMnO_4$ with $MnCl_2$. The sulfide groups in structure of the polymer layer was oxidated to sulfoxide through the formation of MnO_2 NPs. Each step of the catalyst preparation procedure was monitored using techniques such as FTIR to ensure the presence of new functional groups.
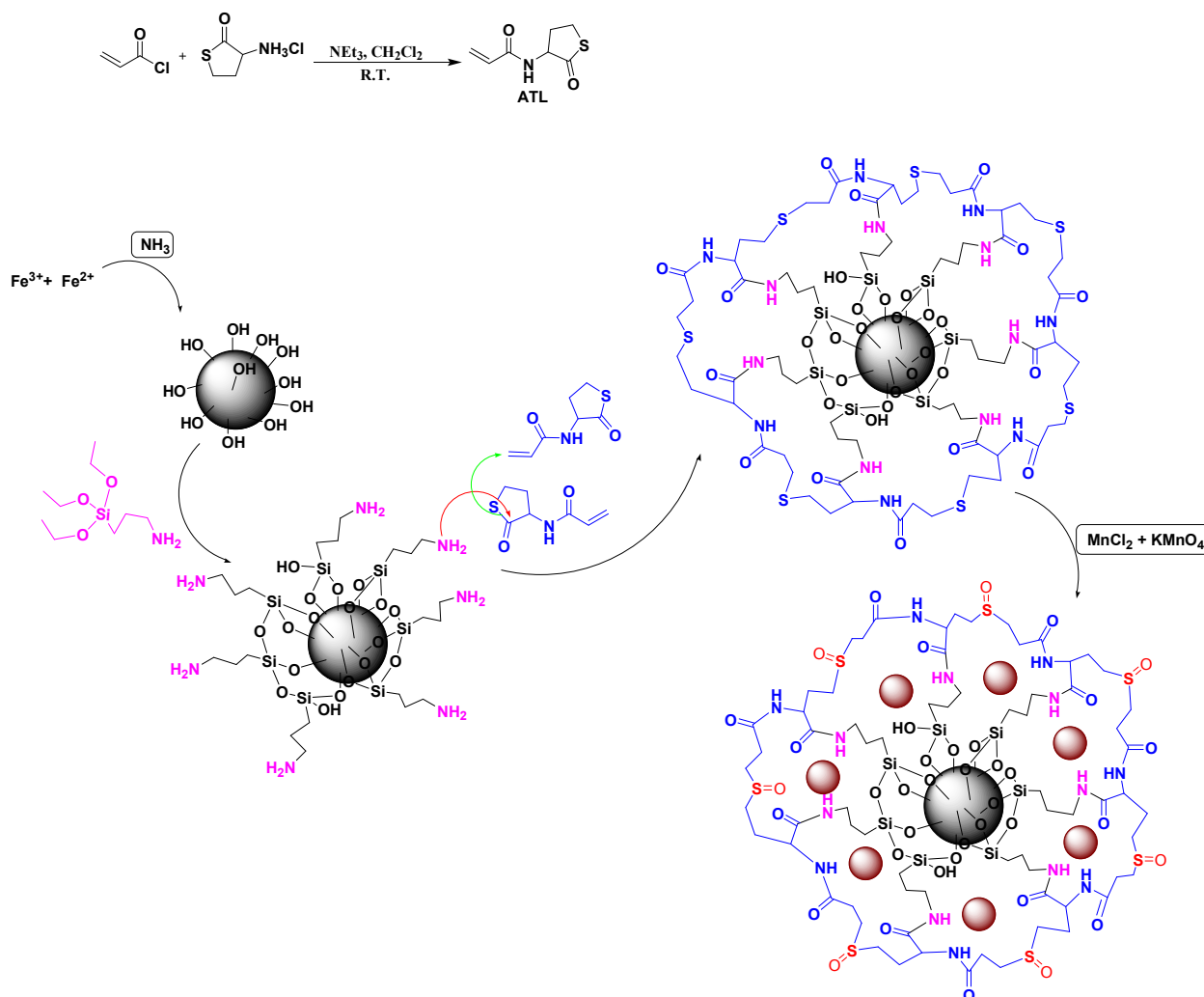
Scheme 1 The schematic pathway for synthesis of $Fe_3O_4/SiO_2/PATL/MnO_2$ nanocatalyst.

The stages of the catalyst formation were tracked by FTIR spectroscopy. Fig. 1 shows the FTIR spectra of the $Fe_3O_4/SiO_2–NH_2$, $Fe_3O_4/SiO_2/PATL$ and $Fe_3O_4/SiO_2/PATL/MnO_2$. The peaks appearing at 645, 591 and 445 cm^{-1} are ascribed to the stretching vibrations of Fe–O bonds, while the absorption peak at 3253 cm^{-1} is the OH stretching vibration characteristic peak, indicating the presence of some amount of ferric hydroxide in Fe_3O_4. At room temperature, Fe^{2+} and Fe^{3+} are converted into hydroxide compounds with a pH above 10 (required pH for magnetite preparation is 11), while at elevated temperature (e.g.60 ^oC within magnetite preparation) they are crystallized to Fe_3O_4 slowly. Silica-coated Fe_3O_4 is expected to produce a corresponding peak of Fe–O–Si bonds at 584 cm^{-1} resulting from the adsorption of silica on the magnetite surface, while this band was overlapped with the Fe–O vibration. In other words, the

formation of Fe–O–Si bonds upon silica coating affected the position of Fe–O bands, and a peak shift occurred. The Si–O–Si stretching and bending vibrations appeared at 1088 and 463 cm^{-1}, respectively.[26] The absorption bands at 3460, 1100 and 960 cm^{-1} are attributed to the stretching, asymmetric stretching, and bending of silanol groups (Si–OH) on the silica surface, respectively. Vibrations at 3500–3400, 1637 and 800 cm^{-1} correspond to the adsorbed water (H–OH, stretching vibration), residual intermolecular water (H–OH, bending), and moisture (H–OH, bending) in the samples. The spectrum of the $Fe_3O_4@SiO_2–NH_2$ shows peaks at 2847 cm^{-1} and 2926 cm^{-1} due to C–H bonds of aliphatic chain stretching vibrations, while the two broad bands at 1580 and 3403 cm^{-1} are attributed to the N–H stretching and bending vibrations, respectively.[27] For the $Fe_3O_4/SiO_2/PATL$ sample, the bond in the range of 1670-1690 cm^{-1} was assigned to the C=O of the amide. After immobilization of MnO_2 NPs onto surface of NPs, the position of C=O and N-H bands was changed due to interaction of MnO_2 NPs with amide's nitrogen. The C=O stretching vibration was observed to shift to 1706 cm^{-1} and the N-H bending vibration appeared at 1530 cm^{-1}.[28] The spectrum of $Fe_3O_4/SiO_2/PATL/MnO_2$ shows a new peak at 1030, which was confirmed the S=O bonds.[29] Therefore, CHN, EDX and TGA analyses were required to confirm the functionalization processes and the presence of polymer layers and MnO_2 NPs on the surface.
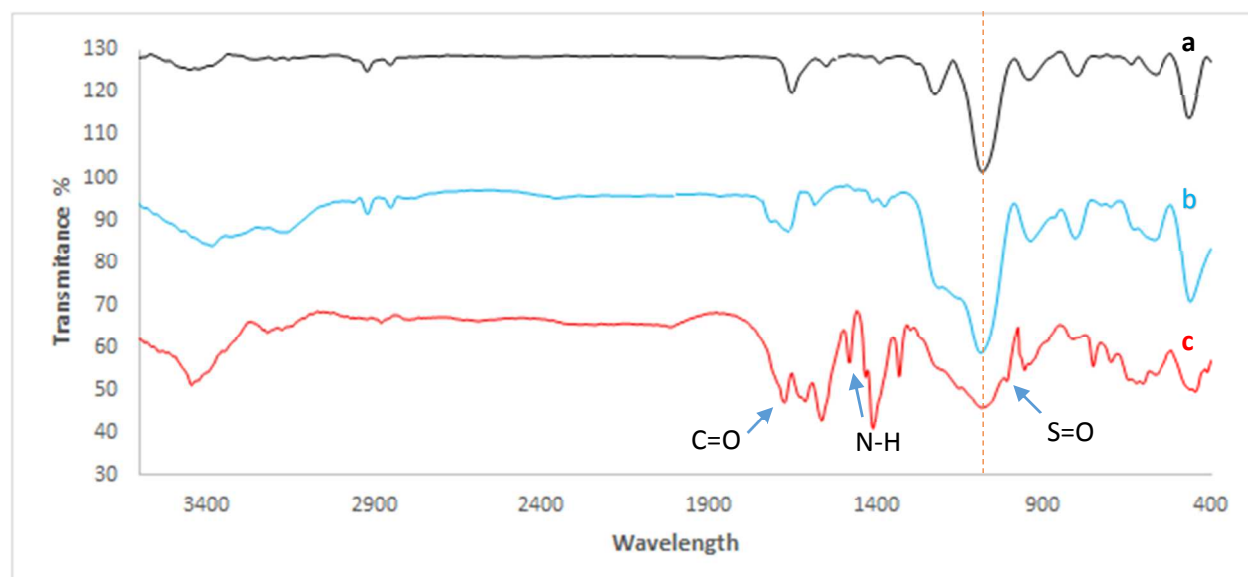

Figure 1 FTIR spectra of the (a) $Fe_3O_4/SiO_2–NH_2$, (b) $Fe_3O_4/SiO_2/PATL$ and (c) $Fe_3O_4/SiO_2/PATL/MnO_2$.

Figure 2 shows the XRD spectra of $Fe_3O_4/SiO_2/PATL$ and $Fe_3O_4/SiO_2/PATL/MnO_2$. The appearance of Fe_3O_4 peaks at 30.1, 35.4, 43.2, 53.6, 57.2 and 62.9 in both spectra indicates the retention of the crystalline structure of Fe_3O_4 through the functionalization steps.[30] As for the XRD patterns of $Fe_3O_4/SiO_2/PATL/MnO_2$, a characteristic peaks at 2θ of, 25.77 and 34.57 are also observed that corresponded to manganese oxide NPs.[31]
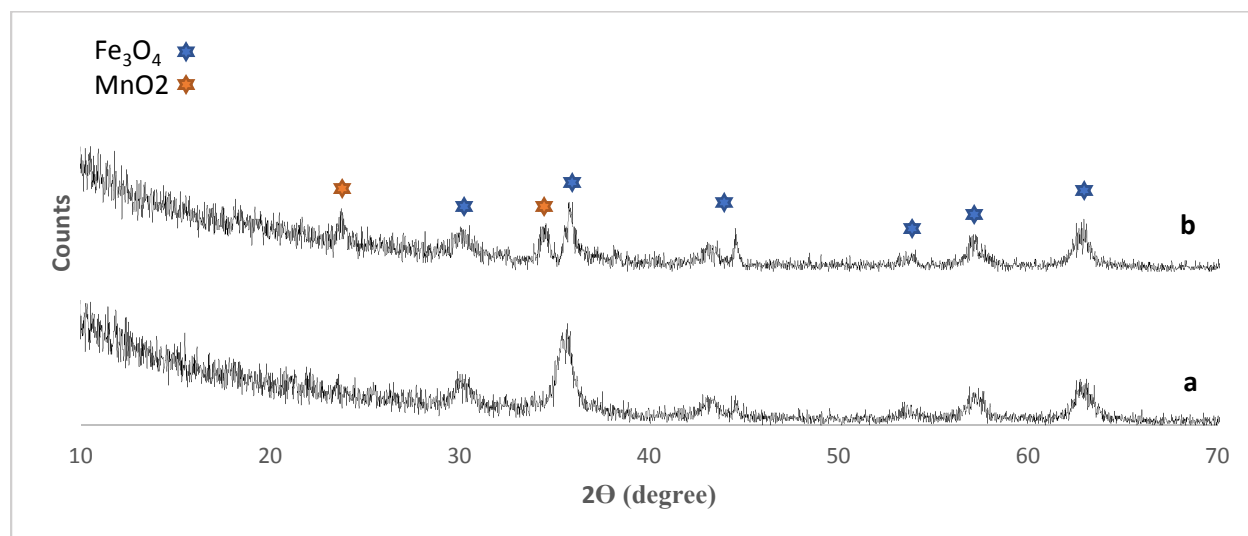

Figure 2 XRD patterns of (a) $Fe_3O_4/SiO_2/PATL$ and (b) $Fe_3O_4/SiO_2/PATL/MnO_2$.

The corresponding TEM image of the magnetite nanoparticles is presented in Figure 3a-d. As seen in this figure, magnetite nanoparticles are spherical with diameter from 70 to 80 nm. The Fe_3O_4 particles have a diameter ranged from 10 to 15 nm and possess regular sphere shape. After coating the magnetite clusters cores with SiO_2 layer, core–shell nanocomposite structured $Fe_3O_4@SiO_2-NH_2$ nanospheres with a thin silica layer of 20 nm in thickness were obtained. These images reveal that the magnetic silica nanoparticles and $Fe_3O_4/SiO_2/PATL$ are similar in size and are spherical in shape. A comparison between TEM images of $Fe_3O_4/SiO_2/PATL/MnO_2$ and previous step revealed that dispersion of MnO_2 NPs is excellent onto the surface of nanocomposites. These particles have a diameter ranged from 10 to 15 nm. In the SEM images, the MnO_2 NPs cannot be clearly seen due to the lower particle size of the MnO_2 NPs than nanocomposites sphere. These SEM images show the granular and spherical morphology for these nanoparticles and the average size of 70 to 80 nm obtained by SEM analysis is consistent with the TEM results (Figure 3e, f).
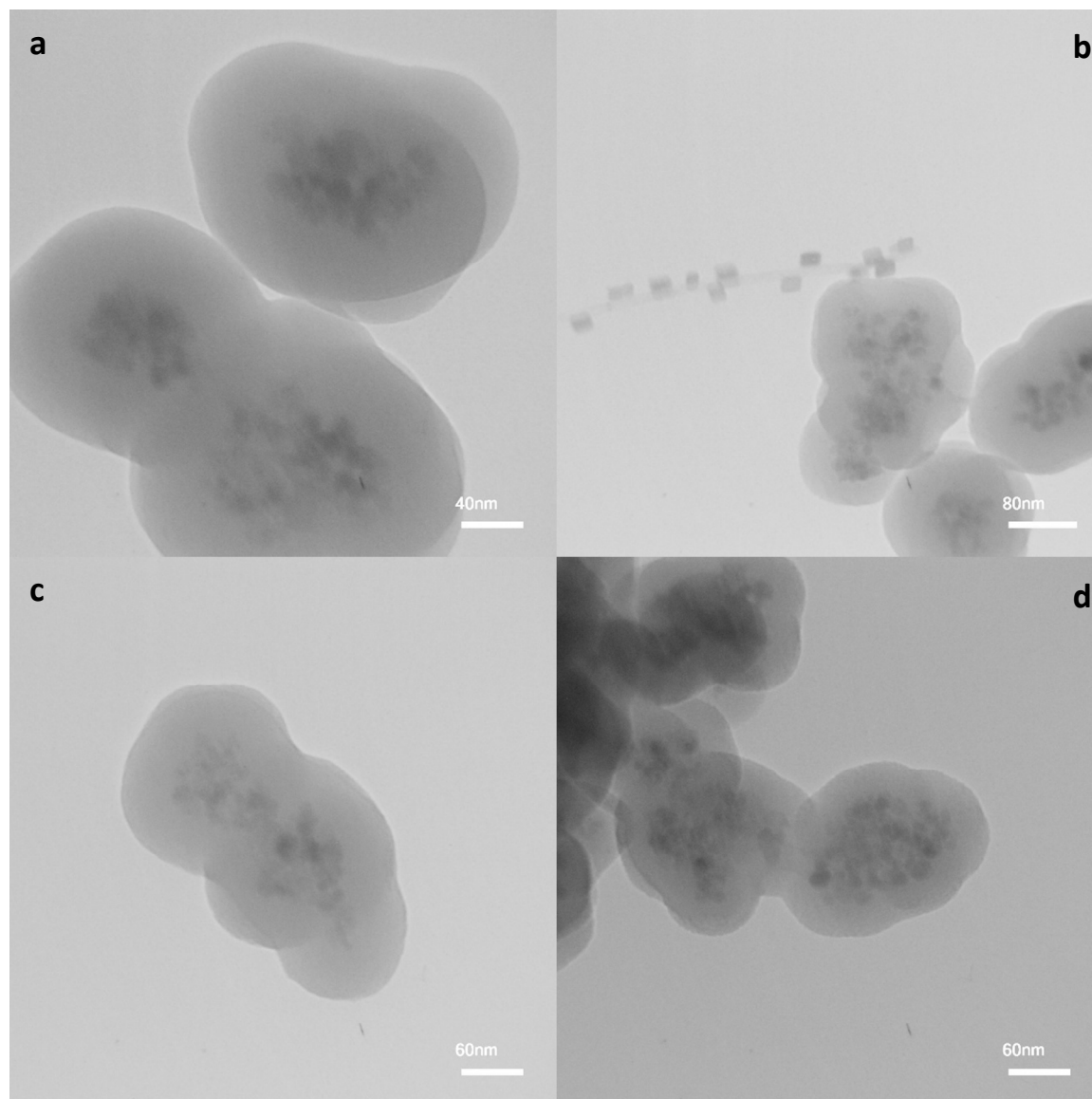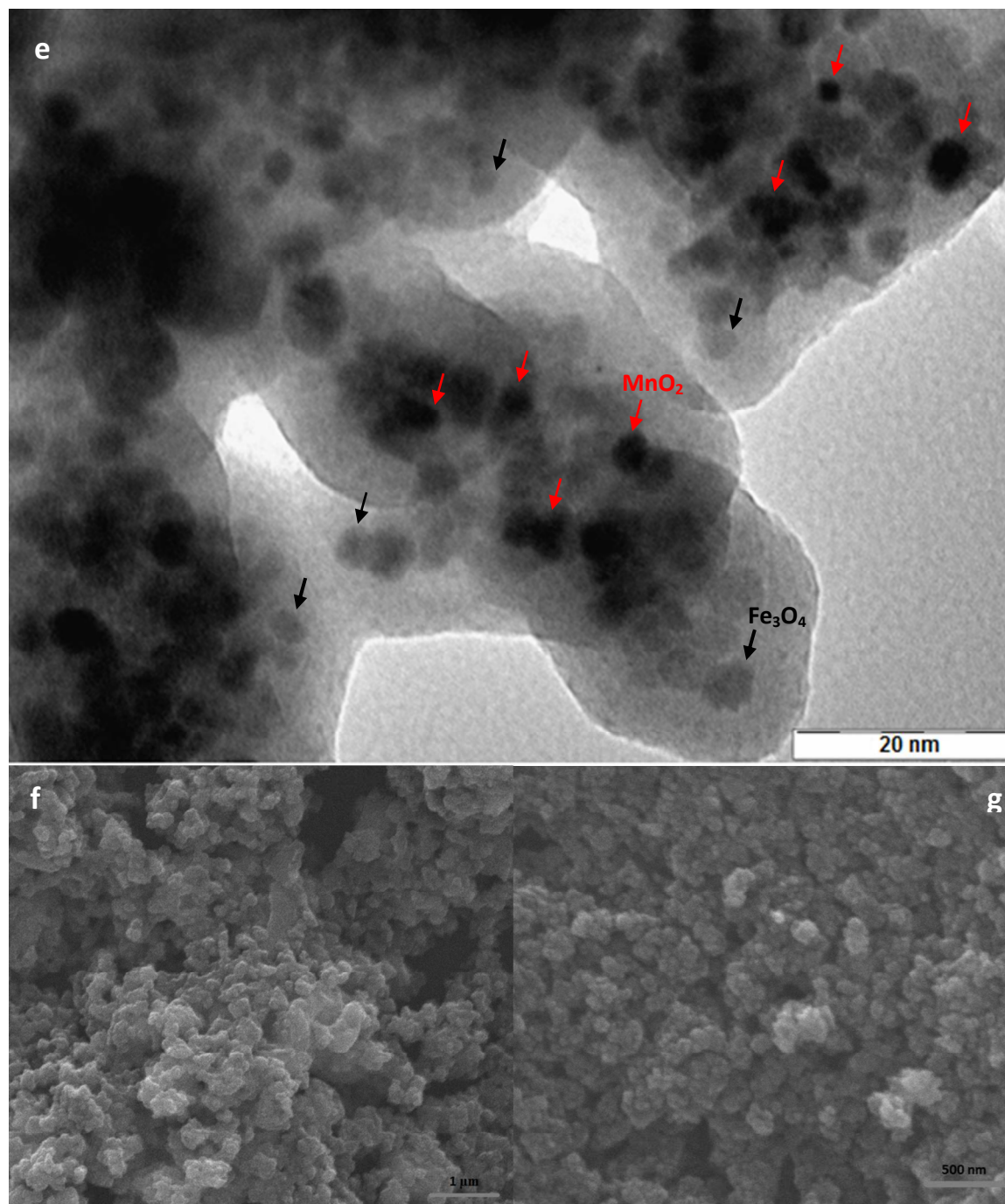
Figure 3 TEM images of (a) $Fe_3O_4/SiO_2–NH_2$, (b, c) $Fe_3O_4/SiO_2/PATL$ and (d, e) $Fe_3O_4/SiO_2/PATL/MnO_2$ (f, g) the SEM images of $Fe_3O_4/SiO_2/PATL/MnO_2$

From the elemental analysis (CHN) in Table 1, it is observed that there is an increase in carbon content and also in hydrogen and nitrogen content after functionalization of the $Fe_3O_4/SiO_2–NH_2$ through the polymerization process. This indicates the successful attachment of organic fragments onto the surface of the nanocomposites. However, the $Fe_3O_4/SiO_2/PATL/MnO_2$ shows

a slightly decrease in the carbon content and also in hydrogen and nitrogen content than $Fe_3O_4/SiO_2/PATL$ due to increase the inorganic content of nanocomposites after formation of MnO_2 NPs on the surface (Table 1). Furthermore, the Energy dispersive X-ray spectroscopy (EDX) in Figure 4 confirmed the presence of polymer layers and MnO_2 NPs on the surface with elemental analysis Fe (60.41%), Si (8.13%), O (17.86%), C (4.26%), N (1.91%), Mn (6.30%), and S (1.13%).

Table 1 the elemental analysis (CHN) result

Elements (mg/g)	$Fe_3O_4/SiO_2–NH_2$	$Fe_3O_4/SiO_2/PATL$	$Fe_3O_4/SiO_2/PATL/MnO_2$
N	4.124	8.734	6.652
C	26.232	36.547	30.916
H	2.071	4.731	3.804
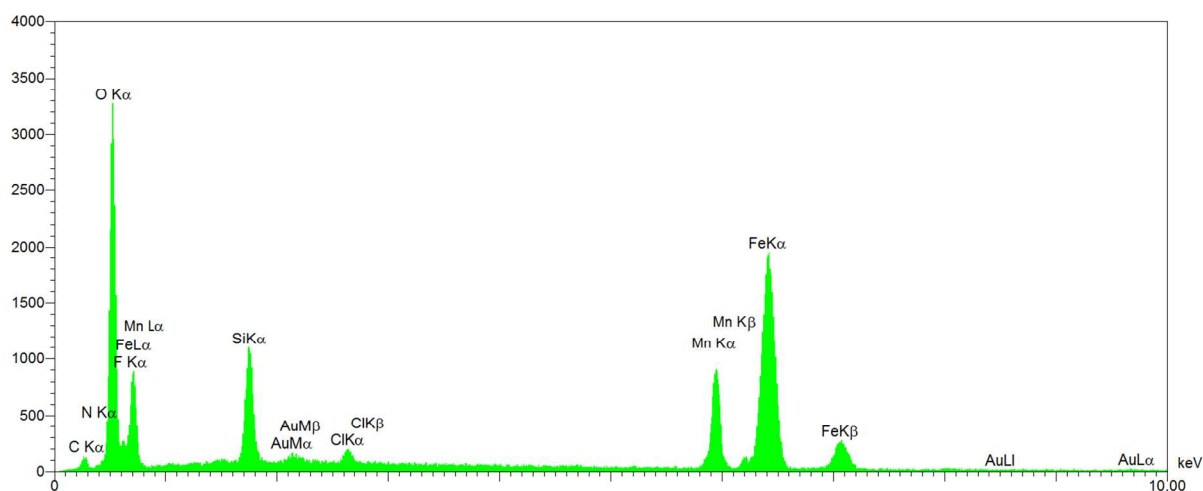
Figure 4 EDX analysis of $Fe_3O_4/SiO_2/PATL/MnO_2$.

Thermogravimetric analysis (TGA) of $Fe_3O_4/SiO_2–NH_2$, $Fe_3O_4/SiO_2/PATL$ and $Fe_3O_4/SiO_2/PATL/MnO_2$ are presented in Figure 5. The initial wt% losses below 150 °C are related to the adsorbed moisture in the samples. The decomposition temperature, which started at 412 °C, and continued until 550 °C, is associated with the decomposition of the organic chains. The organic species decomposed completely at temperatures higher than 600 °C and the residual weights of $Fe_3O_4/SiO_2–NH_2$, $Fe_3O_4/SiO_2/PATL$ and $Fe_3O_4/SiO_2/PATL/MnO_2$ were 90% and

85% and 87%, respectively, at 700 $^{\circ}$C. In other words, the results demonstrate percentages of 4%, 10% and 8% for organic groups on the surface of nanocomposites. The differences between $Fe_3O_4/SiO_2–NH_2$, and $Fe_3O_4/SiO_2/PATL$ confirm the successful plolymerization of ATL on the surface of Fe_3O_4/SiO_2-NH_2 NPs. Also, the TGA curve of $Fe_3O_4/SiO_2/PATL/MnO_2$ shows a decrease in loss of weight because the inorganic content of NPs increased after formation of MnO_2 NPs on surface of $Fe_3O_4/SiO_2/PATL$.
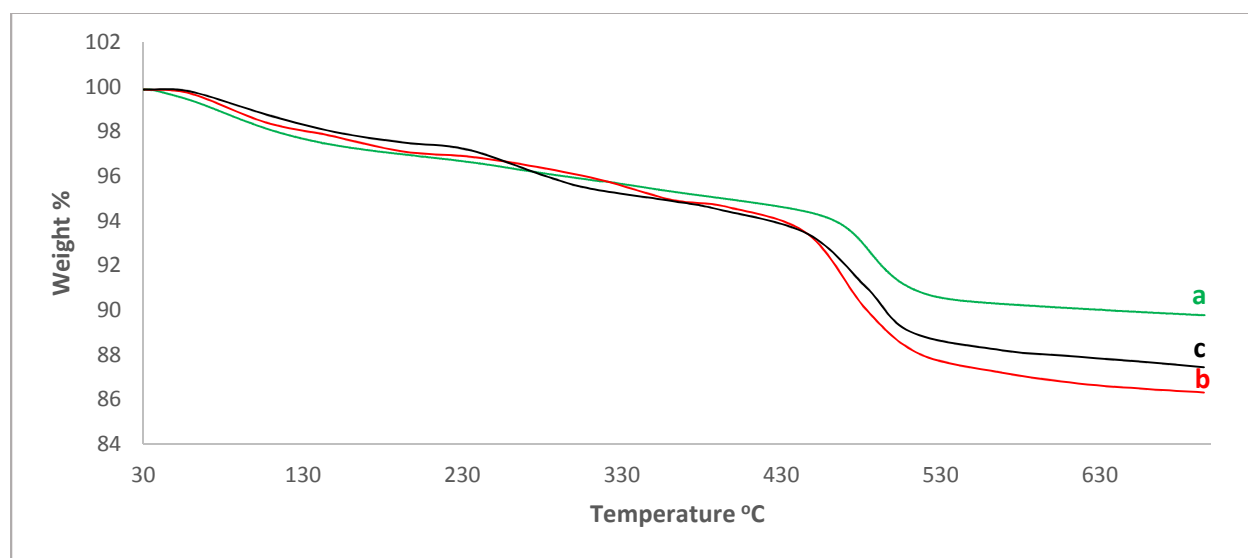

Figure 5 TGA analysis of (a) $Fe_3O_4/SiO_2–NH_2$, (b) $Fe_3O_4/SiO_2/PATL$ and (c) $Fe_3O_4/SiO_2/PATL/MnO_2$.

3.2. Evaluation of the catalytic activity of $Fe_3O_4/SiO_2/PATL/MnO_2$ through the selective oxidation alcohols to corresponding aldehydes and ketones.

In order to optimize the reaction conditions, oxidation of benzylalcohol was selected as a model reaction and various medium such as catalyst amount, solvent and base amount applied to investigate the best medium for selective oxidation primary alcohols to aldehydes. (Table 2). The comparison of the results related to the use of polar and nonpolar solvents that the efficiency of DMSO was higher than other solvents; the reaction yield was 70% after 30 min at 60 $^{\circ}$C. It was found that addition of water to the DMSO solution can improve the reaction outcome and interestingly (entries 10, 11) when the reaction was performed in DMSO/water mixture (1:1) the corresponding product was obtained qualitatively (entry 11) The order of activity of different solvents have been shown in Table 2 (Entries 1-9). It is important to note that the aerobic oxidation of benzylalcohol did not proceed well efficiently without air blowing and the

benzaldehyde was produced about 56% after 3 h stirring at room temperature. Furthermore, effect of various inorganic base was examined on the reaction yields, as well. Based on these experiments K_2CO_3 was found as the preferred inorganic base. Also, different amount of the K_2CO_3 was used to obtain the preferred amount of it (Entries 13-17). To illustrate the need for catalyst, the feasibility of model reaction is checked in the absence of catalyst. No product was obtained at 60 ^{o}C after 12 h. The desired product was scarcely obtained in the presence of $Fe_3O_4/SiO_2-NH_2/PATL$ as catalyst. However, the MnO_2 NPs and MnO_2-immobilized Fe_3O_4/SiO_2-NH_2 were employed in model reaction under optimum conditions, which were obtained moderate yields within 1h. This further confirms the effect of the polymer layer on the catalytic activity of MnO_2 NPs. The main benefit of the polymeric shell seems to come from increased the interaction of nanocomposites with substrates by the hydrogen bands and dipole-dipole interactions. The results showed that the $Fe_3O_4/SiO_2/PATL/MnO_2$ had high dispersibility in compared to MnO_2 and $Fe_3O_4/SiO_2{\sim}NH_2$ under reaction conditions. Additionaly, interactions between metal d orbital and π-level of part of polymer's amide can effect on the delocalization of the electron density over both metal and ligand. These interactions may change the electrochemical properties of metal.[32,33]

Table 2 Optimization of the reaction conditions[a] for aerobicoxidation of alcohols
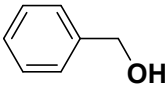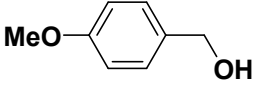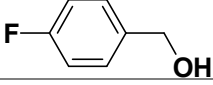
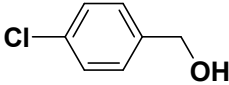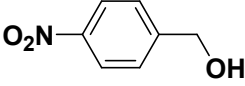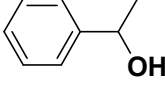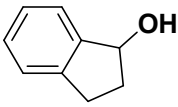| Entry	Catalyst	Amount of catalyst (mol%)	Solvent	Base (mmol)	Yield (%)[b]
1	$Fe_3O_4/SiO_2/PATL/MnO_2$	0.06 g (4.8)	Toluene	K_2CO_3 (0.5)	37
2	$Fe_3O_4/SiO_2/PATL/MnO_2$	0.06 g (4.8)	n-Hexane (r.t.)	K_2CO_3 (0.5)	trace
3	$Fe_3O_4/SiO_2/PATL/MnO_2$	0.06 g (4.8)	Acetonitrile	K_2CO_3 (0.5)	46
4	$Fe_3O_4/SiO_2/PATL/MnO_2$	0.06 g (4.8)	Dichloroethan	K_2CO_3 (0.5)	50
5	$Fe_3O_4/SiO_2/PATL/MnO_2$	0.06 g (4.8)	o-Xylene	K_2CO_3 (0.5)	58
6	$Fe_3O_4/SiO_2/PATL/MnO_2$	0.06 g (4.8)	DMF	K_2CO_3 (0.5)	60
7	$Fe_3O_4/SiO_2/PATL/MnO_2$	0.06 g (4.8)	Water	K_2CO_3 (0.5)	30
8	$Fe_3O_4/SiO_2/PATL/MnO_2$	0.06 g (4.8)	Ethanol	K_2CO_3 (0.5)	35
9	$Fe_3O_4/SiO_2/PATL/MnO_2$	0.06 g (4.8)	DMSO	K_2CO_3 (0.5)	70
10	$Fe_3O_4/SiO_2/PATL/MnO_2$	0.06 g (4.8)	DMSO/Water (2:1)	K_2CO_3 (0.5)	78
11	$Fe_3O_4/SiO_2/PATL/MnO_2$	0.06 g (4.8)	DMSO/Water (1:1)	K_2CO_3 (0.5)	92
12	$Fe_3O_4/SiO_2/PATL/MnO_2$	0.03 g (2.4)	DMSO/Water	K_2CO_3 (0.5)	54
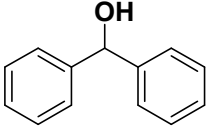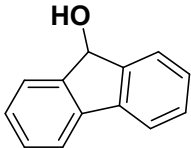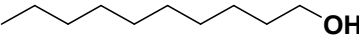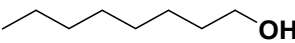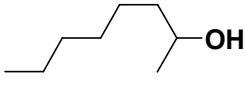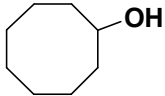
			(1:1)		
13	Fe$_3$O$_4$/SiO$_2$/PATL/MnO$_2$	0.1 g (8)	DMSO/Water (1:1)	K$_2$CO$_3$ (0.5)	88
14	Fe$_3$O$_4$/SiO$_2$/PATL/MnO$_2$	0.06 g (4.8)	DMSO/Water (1:1)	K$_2$CO$_3$ (0.1)	92
15	Fe$_3$O$_4$/SiO$_2$/PATL/MnO$_2$	0.06 g (4.8)	DMSO/Water (1:1)	K$_2$CO$_3$ (0.3)	81
16	Fe$_3$O$_4$/SiO$_2$/PATL/MnO$_2$	0.06 g (4.8)	DMSO/Water (1:1)	NaOAc (1)	50
17	Fe$_3$O$_4$/SiO$_2$/PATL/MnO$_2$	0.06 g (4.8)	DMSO/Water (1:1)	Et$_3$N (1)	58
18	MnO$_2$ NPs	0.006 g (7)	DMSO/Water (1:1)	K$_2$CO$_3$ (0.5)	43
19	Fe$_3$O$_4$/SiO$_2$-NH$_2$/ MnO$_2$	0.06 g	DMSO/Water (1:1)	K$_2$CO$_3$ (0.5)	68
20	Fe$_3$O$_4$/SiO$_2$/PATL	0.06 g	DMSO/Water (1:1)	K$_2$CO$_3$ (0.5)	trace

[a] Reaction conditions: benzylalcohol (1.0 mmol), solvent (5 mL), air oxidant, 60 °C, 30 min. [b] Yield determined by GC analysis.

Subsequently, to investigate the efficiency and applicability of this catalyst in the aerobic oxidation of alcohols to aldehydes and ketones, the reaction was extended to other primary and secondry alcohols at 60 °C in mixture of DMSO/Water (1:1) in presence of K$_2$CO$_3$ (0.5 mmol), as base (Table 3).

Table 3 Selective aerobic oxidation of variuos alcohols to corresponding aldehydes and ketones

Entry	Alcohol	Time (min)	Yield (%)[a]
1		30	92
2		30	90
3		30	89

4		30	90
5		30	93
6		50	93
7		50	92
8		30	94
9		50	89
10		50	82
11		50	84
12		50	80
13		50	90

[a] Yield determined by GC analysis.

3.3. Recyclability of the Fe$_3$O$_4$/SiO$_2$/PATL/MnO$_2$

Recyclability of the Fe$_3$O$_4$/SiO$_2$/PATL/MnO$_2$ was examined in the oxidation reaction of benzylalcohol. For this reason, catalyst which was recovered from reaction using external magnet and reused in the reaction after washed by ethanol and drying under vacuum at 80 °C to 12 h. This procedure was carried out for five repetitive cycles. The results showed that only minor decreases in the reaction yields were observed (Figure 6) and the activity of the catalyst was saved during successive uses.

The concentration of manganese after 5th run measured to be 0.72 mmol g^{-1} by ICP-OES. The TEM micrographs of $Fe_3O_4/SiO_2/PATL/MnO_2$ recycled after 5th run shows the surfaces of nanocomposites are covered with MnO_2 NPs with an average size of 12 nm (Figure 7).

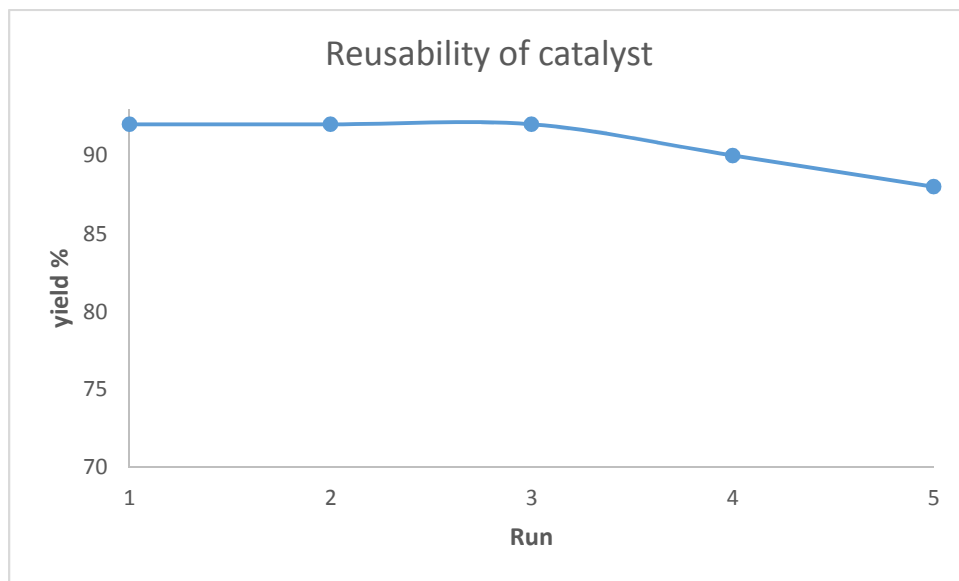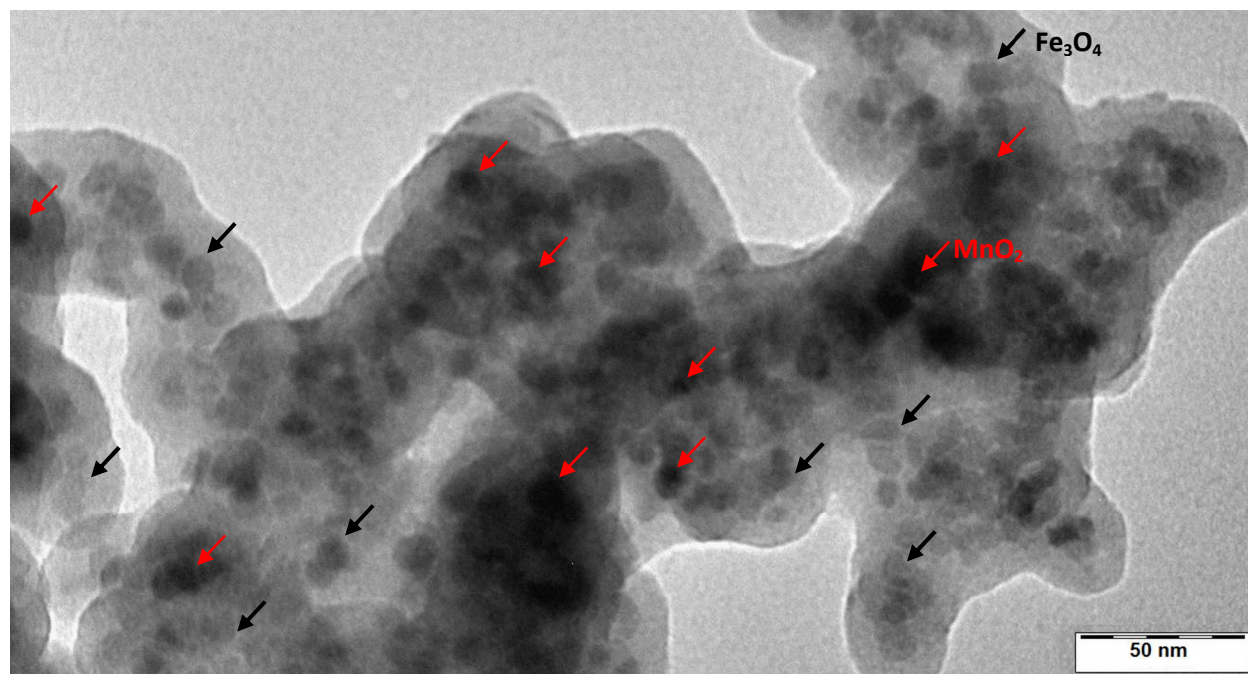**Figure 6** Reusability of the catalyst for the oxidation of the alcohols in 5 run.

Figure 7 TEM images of recycled $Fe_3O_4/SiO_2/PATL/MnO_2$ after 5th run.

4. Conclusions

In this study, synthesis of $Fe_3O_4/SiO_2/PATL/MnO_2$ core/shell nanocomposite was reported. The catalyst was prepared by polymerization of ATL on surface of Fe_3O_4/SiO_2-NH_2 NPs *via* ultrasonic-assisted method and formation of MnO_2 NPs on this surface. The prepared catalysts was characterized *via* FT-IR, XRD, TEM, SEM, EDX, CHN and TGA. The catalytic activity of these catalysts were evaluated in the aerobic oxidation of alcohols to aldehydes and ketones in mixture of DMSO/Water (1:1). The results showed that the $Fe_3O_4/SiO_2/PATL/MnO_2$ had high catalytic activity and selectivity for these reaction.

References

1. M. C. Daniel and D. Astruc, *Chem. Rev.*, 2004,**104**, 293–346.
2. M. B. Gawande, V. D. B. Bonifacio, R. S. Varma, I. D. Nogueira, N. Bundaleski, C. A. A. Ghumman, O. M. N. D. Teodoro and P. S. Branco, *Green Chem.*, 2013, **15**, 1226–1231.
3. A. H. Lu, E. L. Salabas and F. Schuth, *Angew. Chem., Int. Ed.*, 2007, **46**, 1222–1244.
4. V. Georgakilas, A. B. Bourlinos, R. Zboril, T. A. Steriotis, P. Dallas, A. K. Stubos and C. Trapalis, *Chem. Commun.*, 2010, **46**, 1766–1768.
5. V. Georgakilas, M. Otyepka, A. B. Bourlinos, V. Chandra, N. Kim, K. C. Kemp, P. Hobza, R. Zboril and K. S. Kim, *Chem. Rev.*, 2012, **112**, 6156–6214.
6. M. Pykal, K. Safarova, K. M. Siskova, P. Jurecka, A. B. Bourlinos, R. Zboril and M. Otyepka, *J. Phys. Chem. C*, 2013, **117**, 11800–11803.
7. M. Kim, J. C. Park, A. Kim, K. H. Park and H. Song, *Langmuir*, 2012, **28**, 6441–6447.
8. F. Jutz, J. M. Andanson and A. Baiker, *Chem. Rev.*, 2011, **111**, 322–353.
9. C. F. Hoener, K. A. Allan, A. J. Bard, A. Campion, M. A. Fox, T. E. Mallouk, S. E. Webber and J. M. White, J. *Phys. Chem.*, 1992, **96**, 3812–3817.
10. G. H. Yao, F. Wang, X. B. Wang and K. T. Gui, *Energ*, 2010, **35**, 2295-2302.
11. M. Ishii, M. Nakahira and T. Yamanaka. *Solid State Commn.*, 1972, **11**, 209.
12. P. Tartaj, M. P. Morales, T. Gonzalez Carreño, S. Veintemillas Verdaguer and C. J. Serna, *Adv. Mater.*, 2011, **23**, 5243-5249.
13. S. Laurent, D. Forge, M. Port, A. Roch, C. Robic, L. Vander Elst and R. N. Muller, *Chem. Rev.*, 2008, **108**, 2064–2110.

14. X. Gong, S. Peng, W. Wen, P. Sheng and W. Li, *Adv. Funct. Mater.*, 2009, **19**, 292–297.

15. X. Yu, J. Wan, Y. Shan, K. Chen and X. Han, *Chem. Mater.*, 2009, **21**, 4892–4898.

16. L. Wang, C. S. Clavero, Z. Huba, K.J. Carroll, E.E. Carpenter, D. Gu and R. A. Lukaszew, *Nano Lett.*, 2011, **11**, 1237–1240.

17. H. D. She, Y. Z. Chen, X. Z. Chen, K. Zhang, Z. Y. Wang and D. L. Peng, *J. Mater. Chem.*, 2012, **22**, 2757–2765.

18. S. I. Stoeva, K. J. Klabunde, C. M. Sorensen and I. Dragieva, *J. Am. Chem. Soc.*, 2002, **124**, 2305-2309.

19. Y. Qiaozhen, S. Minmin, C. Yunan, W. Mang and C. Hong-zheng, *Nanotechnology.*, 2008, **19**, 265702-265708.

20. C. Guan, X. Xia, N. Meng, Z. Zeng, X. Cao, C. Soci, H. Zhang and H. *J. Fan, Energy Environ. Sci.*, 2012, **5**, 9085–9090.

21. L. Yang, P. W. May and L. Yin, Sequential nucleation and growth of complex nanostructures by a two-step strategy, in *Nanotechnology Nanofabrication, Patterning and Self Assembly,* ed. C. J. Dixon and O. W. Curtines, Nova Science Publishers, Inc., New York, USA, 2010, ch. **12**, pp. 409–433.

22. M. Hakola, A. Kallioinen, M. Kemell, P. Lahtinen, E. Lankinen, M. Leskela, T. Repo, T. Riekkola, M. Siika-aho, J. Uusitalo, S. Vuorela and N. von Wey-marn, *ChemSusChem.,* 2010, **3**, 1142 –1145.

23. R. Rinaldi and F. Schth, *ChemSusChem.*, 2009, **2**, 1096 – 1107.

24. P. Gallezot, *Top. Catal.,* 2010, **53**, 1209 – 1213.

25. Y. Yan, L. Xue, J.B. Miller, K. Zhou, P. Kos, S. Elkassih, L. Liu, A. Nagai, H. Xiong and D. J. Siegwart, *Polymer,* 2015, 1-10.

26. Y. Ahn, E. J. Choi and E. H. Kim, *Rev. Adv. Mater. Sci.*, 2003, **5**, 477–480.

27. S. Ahmad, U. Riaz, A. Kaushik and J. Alam, *J. Inorg. Organomet. Polym.*, 2009, **19**, 355–360.

28. M. Yamaura, R. L. Camilo, L. C. Sampaio, M. A. Macˆedo, M. Nakamura and H. E. Toma, *J. Magn. Magn. Mater.*, 2004, **279**, 210–217.

29. M. Jafarzadeh, E. Soleimani and H. Sepahvand, *RSC Adv.*, 2015, **5**, 42744–42753.

30. M. Jafarzadeh, E. Soleimani, H. Sepahvand, P. Norouzi and R. Adnan. *J. Flu. Chem.,* 2015, **178**, 219-224.

31. L. Zhou, J. He, J. Zhang, Z. He, Y. Hu, C. Zhang and H. He, *J. Phys. Chem.,* C, 2011, **115**, 16873-16878.

32. S. I. Gorelsky, E. S. Dodsworth, A. B. P. Lever and A. A. Vlcek, *Coord. Chem. Rev.*, 1998, **174**, 469-494.

33. J. R. Kitchin, J. K. Nørskov, M. A. Barteau and J. G. Chen, *Phys. Rev. Lett.*, 2004, **93**, 156801-156804.